Histol Histopathol (2009) 24: 879-891

http://www.hh.um.es

Histology and Histopathology

Cellular and Molecular Biology

Immunohistopathological and neuroimaging characterization of murine orthotopic xenograft models of glioblastoma multiforme recapitulating the most salient features of human disease

E. Radaelli[1], R. Ceruti[2], V. Patton[2], M. Russo[2], A. Degrassi[2], V. Croci[2], F. Caprera[2], G. Stortini[2], E. Scanziani[1], E. Pesenti[2] and R. Alzani[2]

[1]Department of Veterinary Pathology, Hygiene and Public Health, Section of Veterinary and Avian Pathology, Faculty of Veterinary Medicine, Milano, Italy and [2]Department of Pharmacology, Nerviano Medical Sciences S.r.l., Nerviano, Italy

Summary. Tumorigenesis in human glioblastoma multiforme (GBM) is driven by several genetic abnormalities with disruption of important molecular pathways, such as p53/MDM2/p14^{ARF} and EGFR/PTEN/Akt/mTOR. The malignant progression of human GBM is also primarily associated with a peculiar multistep pathophysiological process characterized by intratumoral ischemic necrosis (i.e. pseudopalisading necrosis) and activation of the hypoxia-inducible factor (HIF)-1α pathway with consequent peritumoral microvascular proliferation and infiltrative behaviour. Predictable preclinical animal models of GBM should recapitulate the main pathobiological hallmarks of the human disease. In this study we describe two murine orthotopic xenograft models using U87MG and U251 human cell lines. Ten Balb/c nude male mice were orthotopically implanted with either U87MG (5 mice) or U251 (5 mice) cell lines. Intracranial tumor growth was monitored through Magnetic Resonance Imaging (MRI). Immunohistopathological examination of the whole cranium was performed 30 days after implantation. U251 orthotopic xenografts recapitulated the salient pathobiological features described for human GBM, including invasive behaviour, wide areas of pseudopalisading necrosis, florid peripheral angiogenesis, GFAP and vimentin expression, nonfunctional p53 expression, striking active-caspase-3 and HIF-1α expression along pseudopalisades. U87MG orthotopic xenografts proved to be very dissimilar from human GBM, showing expansile growth, occasional necrotic foci without pseudopalisades, intratumoral lacunar pattern of angiogenesis, lack of GFAP expression, fuctional p53 expression and inconsistent HIF-1α expression. Expression of pAkt was upregulated in both models. The results obtained suggest that the U251 orthotopic model may be proposed as a predictive and reliable tool in preclinical studies since it recapitulates the most salient pathobiological features reported for human GBM.

Key words: Glioblastoma multiforme, Hypoxia-inducible factor-1, Mouse model, Pseudopalisading necrosis

Offprint requests to: Alzani Rachele, BU Oncology, Pharmacology Dept, Nerviano Medical Sciences, Viale Pasteur, 10 - 20014, Nerviano (Milan), Italy. e-mail: Rachele.Alzani@nervianoms.com

Introduction

Glioblastoma multiforme (GBM) is the most common and highest grade primary brain tumor that generally arises in the cerebral hemispheres (Kleihues et al., 2000). GBM is divided into those that develop from astrocytic tumors of lower malignancy grade (secondary GBM), such as diffuse astrocytomas [World Health Organization (WHO) grade II] or anaplastic astrocytomas (WHO grade III), and those that develop *de novo*, without evidence of a less malignant precursor lesion (primary GBM) (Ohgaki and Kleihues, 2007). Whether arising de novo or from a lower-grade precursor GBM has a truly dismal prognosis with rapid clinical progression leading ultimately to death (Mischel et al., 2003; Brat and Van Meir, 2004). The main biologic properties that make GBM fatal are poor response to a series of adjuvant therapies and infiltrative behaviour that makes complete surgical resection nearly

impossible (Brat et al., 2004).

Specific genetic abnormalities such as LOH 10q, TP53 mutation, PTEN mutation, p16INK4a deletion and EGFR amplification-overexpression are common in GBM. These genetic aberrations account for a series of disrupted molecular pathways (i.e. p53/MDM2/p14^{ARF} pathway; p16^{INK4a}/RB1 pathway; EGFR/PTEN/Akt/mTOR pathway) that regulate vital cellular processes, including apoptosis, cell proliferation and cell migration (Ohgaki and Kleihues, 2007). The development of GBM is also primarly associated with a peculiar multistep pathophysiological process that links intratumoral ischemic necrosis (i.e. pseudopalisading necrosis) and hypoxia to angiogenesis and infiltrative behaviour (Brat et al., 2004; Rong et al., 2006). Pseudopalisading necrosis is basically characterized by an intratumoral serpentine area of coagulative necrosis lined by palisade-oriented GBM cells (pseudopalisades) (Kleihues et al., 2000). Endothelial cell apoptosis in intratumoral vessels and secondary vascular thrombosis contribute to the ischemic necrosis and hypoxic state (Kaur et al, 2004; Preusser et al 2006). In turn, hypoxia stimulates pseudopalisading cells to activate hypoxia-inducible factor (HIF-1α) leading to overexpression of angiogenetic factors and peritumoral microvascular proliferations (Brat et al., 2002, 2004). Hypoxia is also responsible for the highly invasive behaviour of GBM, as it elicits migration of GBM cells away from hypoxic areas (Pennacchietti et al., 2003; Brat et al., 2004). Pseudopalisading necrosis and microvascular hyperplasia currently represent two of the most powerful predictors of poor prognosis in human GBM (Rong et al., 2006).

Tremendous technical advances have allowed the use of Magnetic Resonance Imaging (MRI) as a non-invasive method for detection and diagnosis of primary brain tumors. In astrocytic tumors MRI also gives useful prognostic indications, detecting the early formation of pseudopalisading necrosis and microvascular proliferations during the progression of secondary GBM from lower grade tumor (Goldbrunner et al., 2000). MRI also represents a fundamental tool for monitoring blood-brain barrier permeability and the therapeutic responsiveness of GBM in terms of tumor regression and inhibition of angiogenesis (Zhu et al., 2000; Henson et al., 2005).

Intriguing insights into the pathogenesis of GBM and more accurate prognostic and therapeutic directions are emerging from the contextual examination of clinical, immunohistopathological and genomic features. The study of the biological mechanisms underlying GBM development and the evaluation of new therapies require accurate and reproducible brain tumor animal models. Predictable animal models of GBM should recapitulate the main pathobiological hallmarks of the human disease concerning progression, kinetics and tumor-host interaction. Although rodent orthotopic xenografts of human GBM are widely employed in preclinical research, their use remains controversial and these models have been criticized for not recapitulating the main morphological and biological aspects of human GBM (Fomchenko and Holland, 2006). In fact, recent investigations confirmed that fundamental immuno-histopathological, neuroimaging and biological similarities exist between murine orthotopic xenograft models and naturally occurring human GBM (Candolfi et al., 2007; Martínez-Murillo and Martínez, 2007). A detailed characterization and standardization are therefore mandatory to rule out the predictivity range of specific preclinical models.

In this study, we report the histopathological, immunohistochemical and imaging (MRI) characterization of mouse orthotopic xenograft models using two different cell lines of human GBM, U251 and U87MG.

Material and methods

Cell lines

The human brain tumor cell lines U251 and U87MG (glioblastomas) were purchased from National Cancer Institute, Bethesda, MD and from American Type Cell Culture, Manassas, VA respectively and grown in RPMI1640 medium supplemented with 10% Fetal Calf Serum (FCS), 2 mM L-Glutamine (U251) and Eagle's Minimal Essential Medium (E-MEM) supplemented with 10% FCS, 2 mM L-Glutamine and 1% non-essential amino acids (U87MG).

Animals and study design

All procedures adopted for housing and handling the animals were in strict compliance with EEC and Italian Guidelines for Laboratory Animal Welfare.

Ten Balb/c nude male mice, aged 6-8 weeks, were anesthetized and stereotactically implanted in the putamen region with human GBM cell lines, 5 mice with U87MG and 5 mice with U251 (10^5 cells in 2 µl of PBS).

By using the stereotactic X and Y axis controller, bregma (interception between median sagittal and anterior coronal sutures) and lambda (interception between median sagittal and posterior coronal sutures) were identified as point 0. The following coordinates [+ 1 mm posterior and + 3 mm lateral (right)] were set in the apparatus and the point of injection identified. With a microdrill a small hole was made in the desired point. Cells were aspirated with a Hamilton syringe just prior to injection (a brief mix of cells before aspiration is performed to avoid precipitation of cells). By pointing to the hole, Z axis was fixed to 0 and the syringe gently inserted into the brain until reaching the correct coordinate (-3.5 mm depth). Cells were injected at the speed of 1 µl every minute. The syringe was left for an additional 5 minutes in the hole before removing it to avoid cell aspiration. The hole was closed using bone wax and the wound was closed with sterile autoclips. Following surgery, mice were monitored for recovery until complete wakening.

MR imaging

MRI was performed to visualize and delineate tumors in the nuclei area. In order to monitor tumor progression in each animal, a serial study was perfomed by weekly imaging sessions starting at day 8 after intracranial injection. For imaging studies, mice were anesthetized with gas isofluoran, positioned prone in the animal bed and inserted in the radiofrequency coil (38 mm i.d.) inside the magnet. Images were acquired on a Bruker Pharmascan instrument (Bruker, Germany) equipped with a 7.0 T horizontal magnet. Transversal and sagittal spin echo multislice images were acquired as pilot scans for correct localization of brain areas. Then, T2-weighted (T2-W) and T1-weighted (T1-W) scans were run in both transversal and coronal orientations in order to better highlight the characteristics and location of tumors. T1-W images were acquired before and after iv injection of the contrast agent gadolinium-diethylenetriamine penta-acetic acid (Gd-DTPA, Guerbet). Imaging parameters were as follows:

T2-W: RARE (TR=5000 ms; TEeff=57 ms; rare factor=8; 4 averages; FOV=2.5*2.5 cm^2; Slice thickness=1 mm; matrix=256*128; Total acquisition time=5 min 20sec.

T1-W: RARE (TR=800 ms; TEeff=25.5 ms; rare factor=4; 4 averages; FOV=2.5*2.5 cm^2; Slice thickness=1 mm; matrix=256*128; Total acquisition time=1 min 42sec.

The whole imaging session lasted around 25 minutes for each animal.

Histopathology & Immunohistochemistry

For histopathology and immunohistochemistry studies, mice were sacrificed at a late stage of the disease corresponding more or less to day 30 after intracranial injection. The whole cranium from each animal was collected and fixed in buffered formalin for 4 to 5 hours then decalcified in 5% formic acid diluted in buffered formalin for 24h. The region between external auditory meatus and orbit was sliced and a coronal section of the whole cranium was obtained and embedded in paraffin. Serial 4 μm-thick sections were subsequently placed on Superfrost plus slides and stained with haematoxylin and eosin (HE) for histological examination. For immunohistochemistry, sections were deparaffinized in xylene, rehydrated in graded ethanol, and transferred to PBS. Heat treatment antigen retrieval was performed in citrate buffer pH 6 (Vector). The slides were rinsed with PBS and endogenous peroxidase was blocked using 3% hydrogen peroxide (Sigma) in PBS for 10 minutes. The tissues were incubated for 20 minutes at room temperature with a protein-blocking solution consisting of PBS containing 0.05% Tween 20 (DAKO) and 10% normal goat serum (Vector). Slices were then incubated with the primary antibodies as reported in Table 1. The samples were then rinsed in PBS containing 0,05% Tween 20 and incubated for 30 minutes at room temperature with the appropriate secondary antibody as reported in Table 1. Glial fibrillary acidic protein (GFAP), S100 and Factor VIII (FVIII)-stained slides were additionally incubated for 30 minutes at room temperature with streptavidin-peroxidase (Dako). Finally, the reaction was developed with diaminobenzidine (Dako).

Immunostained and HE-stained sections from each case were qualitatively and quantitatively/semi-quantitatively scored as follow (see also Table 2).

Necrosis (HE stained sections):

(-) = no intratumoral necrotic foci

(+) = <20% of the mass effaced by intratumoral necrotic foci

(++) = 20-50% of the mass effaced by intratumoral necrotic foci

(+++) = >50% of the mass effaced by intratumoral necrotic foci

HIF-1α nuclear expression by neoplastic cells:

(-) = No immunohistochemical expression of HIF-1α by neoplastic cells

(+) = Immunohistochemical expression of HIF-1α by neoplastic cells in perinecrotic areas

(++) = Immunohistochemical expression of HIF-1α by neoplastic cells in perinecrotic areas and in the viable portion of the tumor as well

Tumor-associated thrombi:

Table 1. Antibodies used in immunohistochemical assay: source, clone/company code, dilution, incubation time and secondary antibody.

ANTIBODY	COMPANY	CLONE / COMPANY CODE	WORKING DILUTION	INCUBATION TIME	SECONDARY ANTIBODY
Vimentin	Epitomics	SP20	1:50	40 min at 37°C	EnVision Rabbit-HRP
GFAP	Dako	Z334	1:10000	40 min at 37°C	Biotinylate Anti-Rabbit
S100	Dako	Z311	1:15000	40 min at 37°C	Biotinylated Anti-Rabbit
Synaptophysin	Epitomics	EP1098Y	1:100	1 hour at room temperature	EnVision Rabbit-HRP
HLA-abc	MBL	EMR8-5	1:100	1 hour at room temperature	EnVision Mouse-HRP
FVIII	Dako	N1505	1:80	40 min at 37°C	Biotinylated Anti-Rabbit
Active-caspase-3	Cell Signaling	Asp175	1:100	1 hour at room temperature	EnVision Rabbit-HRP
p53	Dako	DO-7	1:50	1 hour at room temperature	EnVision Mouse-HRP
HIF 1α	BD Transduction Laboratories	54	1:50	1 hour at room temperature	EnVision Mouse-HRP
Ki-67	Dako	MIB-1	1:150	1 hour at room temperature	EnVision Mouse-HRP
AKT (pS473)	Epitomics	EP 2109y	1:200	1 hour at room temperature	EnVision Rabbit-HRP

(-) = no FVIII positive intratumoral thrombi
(+) = <20 FVIII positive intratumoral thrombi
(++) = 20-50 FVIII positive intratumoral thrombi
(+++) = >50 FVIII positive intratumoral thrombi

Tumor angiogenesis (microvessel density):

The number of FVIII positive vascular channels were assessed in four 400x microscopic fields both in the centre and at periphery of the tumor. Mean values from each case are reported (Table 2).

Ki-67 (MIB-1) and p53 expression by neoplastic cells: Both for Ki-67 and p53, the number of immunopositive nuclei were counted on a total amount of about 3000 neoplastic cells at 200x microscopic fields. Mean percentages from each case are reported (Table 2).

Immunohistopathological evaluations were performed using Image Pro-Plus 6.0 software technology. Statistical analysis was performed using Mann-Whitney test (Prism 3.0 software).

Results

Imaging

The development and growth of neoplastic lesions derived from U251 or U87MG implantation were followed in each animal at different time points. Both cell lines grew very quickly, even if a more aggressive growth pattern was noticed in the U251 model.

In terms of MR signal intensity, some differences were observed for the two cell lines. The U251 tumor was delineated from normal brain tissue as an isointense or lightly hyperintense, poorly demarcated, irregularly rounded area surrounded by a hyperintense rim (peritumoral edema). The development of intratumoral necrotic areas was common in this model (Fig. 1a'-d'). The U87MG tumor was delineated from normal brain tissue as a hyperintense, well demarcated, nodular area, with a regularly expansile growth (tennis ball appearance) (Fig. 2a-d). In both models the compression caused by tumor growth leads to internal hydrocephalus, due to blockage of cerebrospinal fluid outflow in the ventricles or in the subarachnoid space (Fig. 1d' and 2d). Gd-DTPA uptake profile in U251 xenograft showed that the tumor was poorly distinguishable in the pre-contrast T1-weighted image (Fig. 3b) and it became gradually hyperintense after iv contrast injection in the tail vein. Irregular signal dishomogeneities were present inside the tumor, due to the presence of necrotic areas. Contrast agent, initially confined in the viable portion of the tumor, gradually accumulated in necrotic regions and diffused in the peritumoral well vascularized and edematous areas (Fig. 3c,d).

Histopathology and immunohistochemistry

U251 orthotopic xenografts were morphologically characterized by a single, densely cellular, irregular, poorly demarcated, unencapsulated, intrahemispheric mass with peripheral medusoid projections invading the

Table 2. The table summarizes the scores for the different histopathological and immunohistochemical aspects investigated in U87MG and U251 murine orthotopic xenograft models of human glioblastoma multiforme.

GBM line	Record	Ki-67	p53*	Angiogenesis*		Necrosis	HIF-1α	Thrombi
				Central	*Peripheral*			
U87MG	#67-1	45.10%	11.61%	9	3.25	-	-	++
	#663-1	41.69%	24.11%	10.5	1.25	++	+	+++
	#851-1	56.78%	11.94%	12	2.25	-	-	+
	#861-1	41.71%	6.94%	9.25	3	+	+	++
	#899-1	32.85%	9.8%	14.5	2.25	-	-	+++
Mean		43.63%	12.88%	11.05	2.4			
U251	#389-1	36.71%	90.12%	0	6.25	++	++	-
	#952-2	47.74%	99.8%	0	7.5	+	++	-
	#966-3	51.48%	99.72%	0.25	10.5	++	++	-
	#9614-3	63.66%	95.43%	0	7.5	+	++	-
	#9615-3	60.35%	97.51%	2	11	+	++	-
Mean		52%	96.51%	0.45	8.55			

* Statistically significant differences between U251 and U87MG group. Necrosis (HE stained sections): (-) = no intratumoral necrotic foci, (+) = <20% of the mass effaced by intratumoral necrotic foci, (++) = 20-50% of the mass effaced by intratumoral necrotic foci, (+++) = >50% of the mass effaced by intratumoral necrotic foci; HIF-1α nuclear expression by neoplastic cells: (-) = No immunohistochemical expression of HIF-1α by neoplastic cells, (+) = Immunohistochemical expression of HIF-1α by neoplastic cells in perinecrotic areas, (++) = Immunohistochemical expression of HIF-1α by neoplastic cells in perinecrotic areas and in the viable portion of the tumor as well; Tumor-associated thrombi: (-) = no FVIII positive intratumoral thrombi, (+) = <20 FVIII positive intratumoral thrombi, (++) = 20-50 FVIII positive intratumoral thrombi, (+++) = >50 FVIII positive intratumoral thrombi; Tumor angiogenesis (microvessel density): The number of FVIII positive vascular channels were assessed in four 400x microscopic fields both in the centre and at periphery of the tumor. Mean values from each case are reported; Ki-67 and p53 expression by neoplastic cells: Both for Ki-67 and p53. the number of immunopositive nuclei were counted on a total amount of about 3000 neoplastic cells at 200x microscopic fields. Mean percentages from each case are reported.

surrounding cerebral parenchyma and often spreading into the controlateral hemisphere. This mass consisted of tightly packed, interlacing bundles of pleomorphic, spindle to stellate cells with occasional giant and multinucleated elements. Findings of atypia, including marked anisocytosis, anysokariosis, bizarre mitosis and multiple irregular nucleoli, were common among neoplastic cells. In all examined cases, wide intratumoral foci of vascular-oriented (serpentine) pseudopalisading necrosis were observed (Table 2; Fig. 4A). Infiltrating neoplastic projections at the periphery of the mass were intimately associated with tortuous microvascular

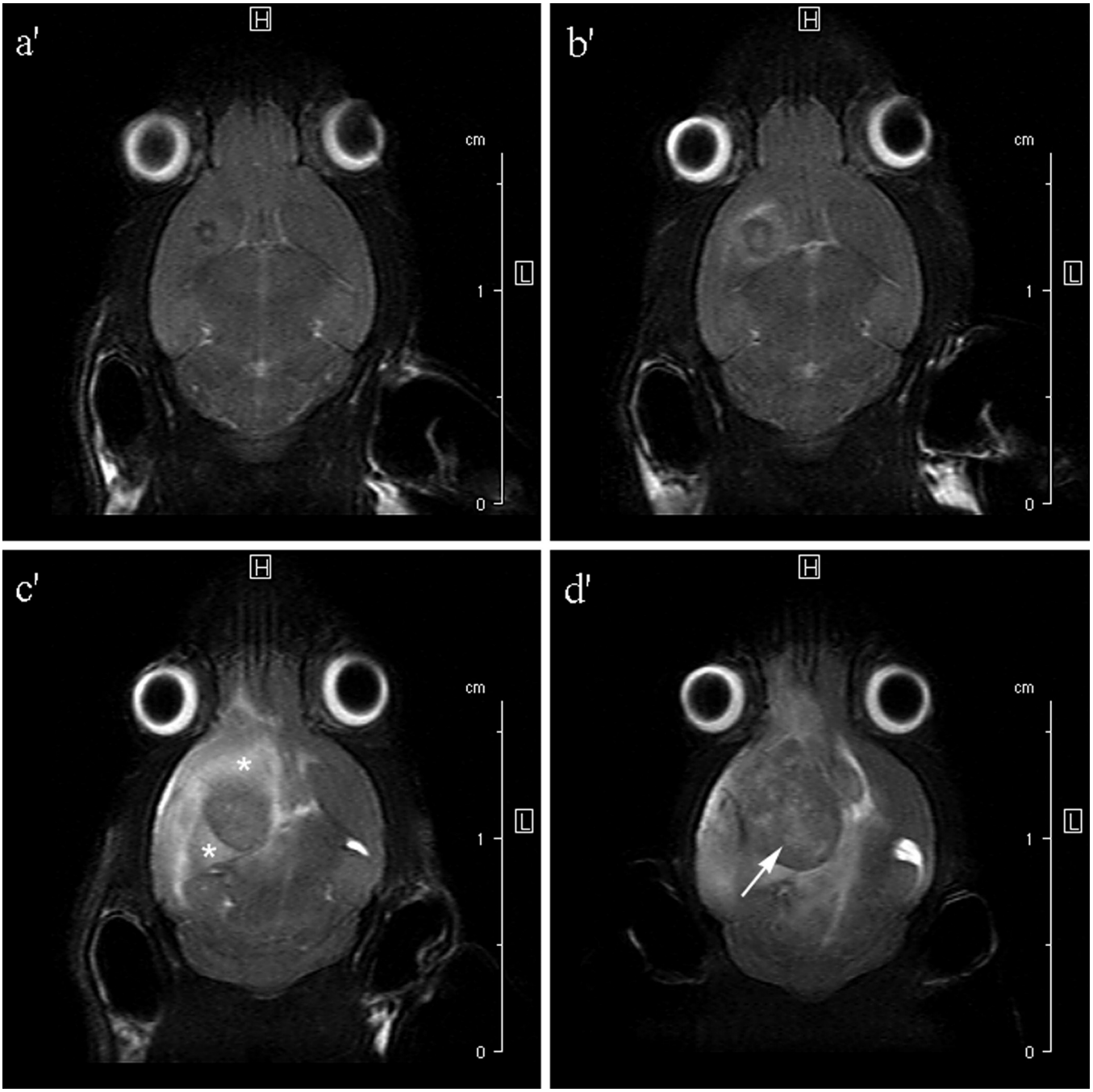

Fig. 1. T2-weighted images: coronal sections at different time points showing the progression and growth of the intrahemispheric neoplastic lesions in U251 (**a':** day 8; **b':** day 15; **c':** day 21; **d':** day 28). U251 xenograft appears as an isointense or lightly hyperintense, poorly demarcated, irregularly rounded area surrounded by a hyperintense rim (peritumoral edema, asterisks). Note also the presence of intratumoral necrosis (arrow).

proliferations often characterized by hypertrophic lining endothelium. Prominent rarefaction-*status spongiosus* and edema of the surrounding neuroparenchyma and occasional intratumoral and peritumoral haemorrhagic foci were also observed. Infiltrating neoplastic extensions along the ependimal surface into the lateral ventricles (Fig. 4B) as well as along the pial surface into the subarachnoid space represented a common finding.

In U251 orthotopic xenografts, almost all the neoplastic cells displayed intense vimentin expression,

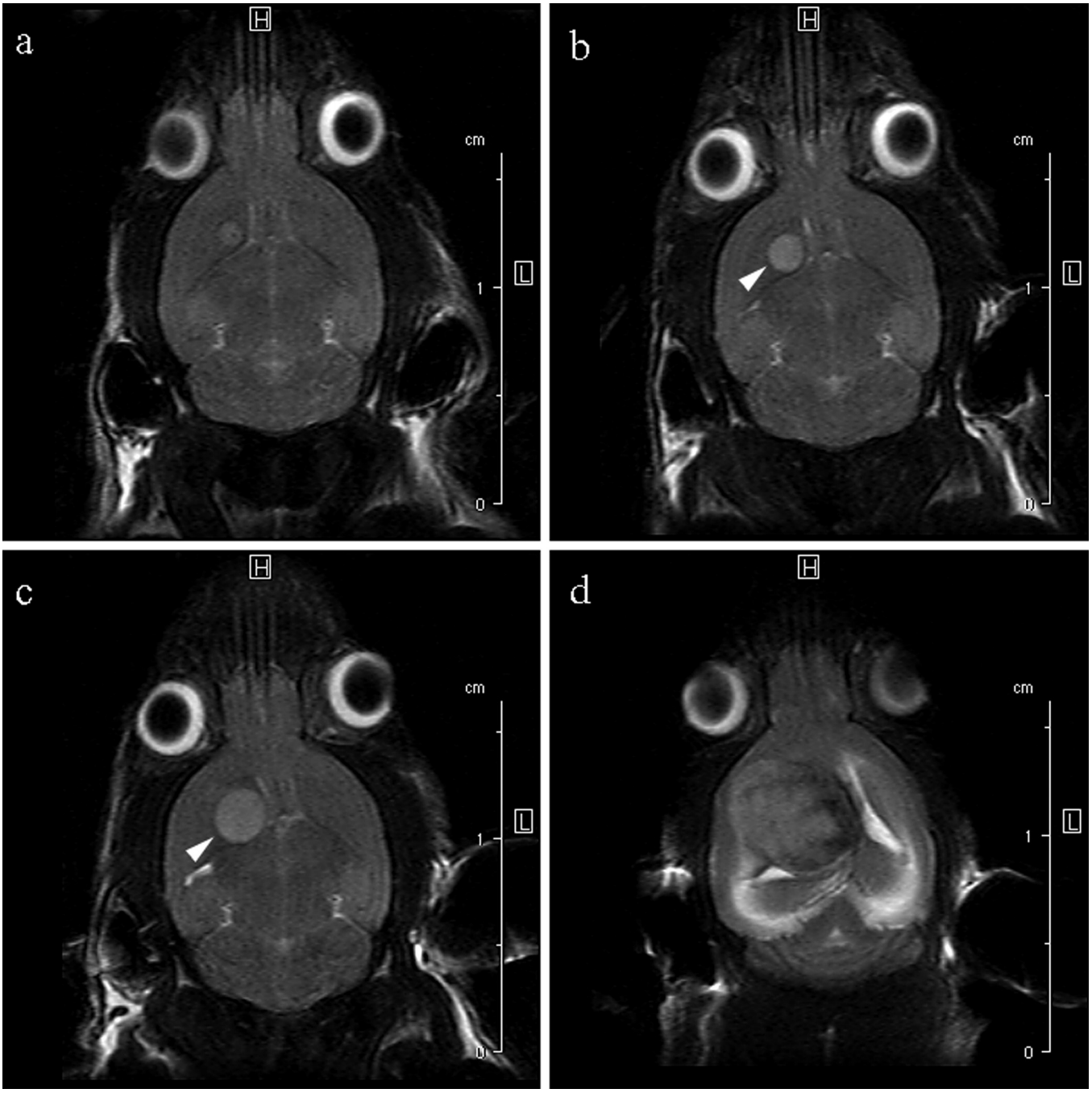

Fig. 2. T2-weighted images: coronal sections at different time points showing the progression and growth of the intrahemispheric neoplastic lesions in U87MG xenografts (**a:** day 8, **b:** day 14, **c:** day 22, **d:** day 29). U87MG xenograft appears as a hyperintense, well demarcated, nodular area, with a regularly expansile growth and a tennis ball appearance (arrowhead).

whereas only 40% and 10% of these cells resulted GFAP and S100 positive respectively (Fig. 4C). GFAP-expression was also observed in the loose and incomplete rim of reactive astrogliosis that surrounded neoplastic structures (Fig. 4C). A diffuse synaptophysin expression was observed in bearing brain parenchyma but not in U251 neoplastic cells. An accurate distinction between U251 neoplastic astrocytes and murine reactive

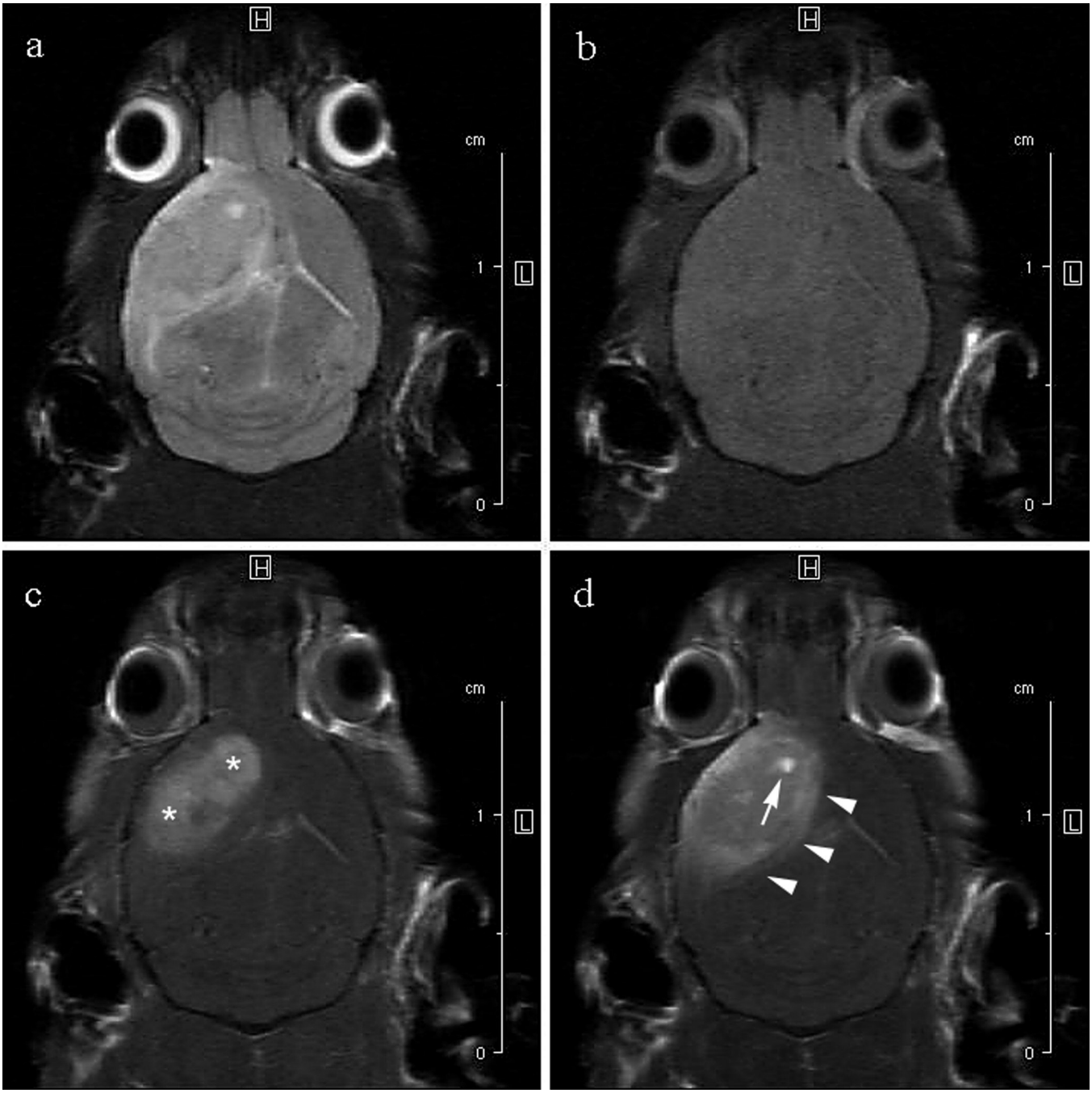

Fig. 3. MR images of a mouse intracranially injected with U251 cell line (day 28). A T2-weighted image (**a**) is compared with T1-weighted images before (**b**) and after (**c, d**) contrast agent injection (**c, d:** 12' and 30' after Gd-DTPA iv injection). U251 tumor is poorly distinguishable in the pre-contrast T1-weighted image and it becomes gradually hyperintense after iv contrast injection. Contrast agent, initially confined in the viable portion of the tumor (asterisks), gradually accumulates in necrotic regions (arrow) and diffuses in the peritumoral well vascularized and edematous areas (arrowheads).

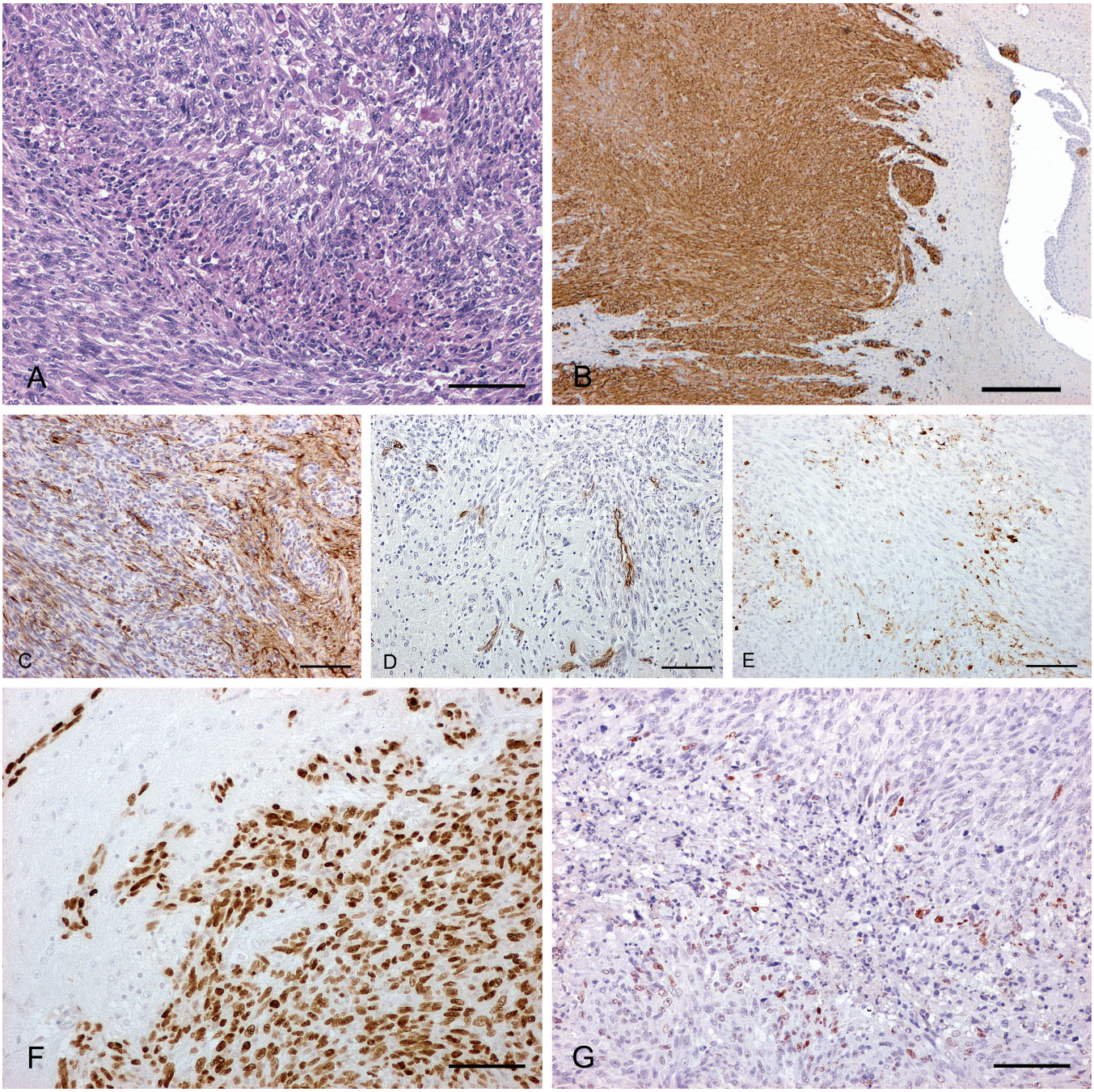

Fig. 4. Histopathology and immunohistochemistry of murine intracranial orthotopic xenograft of glioblastoma multiforme using U251 human cell line. **A.** Linear intratumoral area of pseudopalisading necrosis. HE staining. **B.** The human-specific marker HLA-abc defines the infiltrative projections of intracranial U251 xenograft with invasion of lateral ventricles and spread toward the controlateral hemisphere. HLA-abc immunostaining. **C.** Approximately 40% of the neoplastic cells within the U251 xenograft display GFAP expression. Marked GFAP expression is also evident in the incomplete and loose peripheral rim of astrogliosis. GFAP immunostaining. **D.** Disseminated along the infiltrative medusoid neoplastic projections are numerous FVIII-positive vascular channels. FVIII immunostaining. **E.** Disseminated along the serpiginous intratumoral pseudopalisading necrosis are numerous apoptotic cells. Active caspase-3 immunostaining. **F.** Virtually all neoplastic cells within the U251 xenograft display prominent intranulcear accumulation of p53 protein. p53 immunostaining. **G.** Numerous neoplastic cells with prominent HIF-1α-nuclear expression are concentrated along an intratumoral area of pseudopalisading necrosis. HIF-1α immunostaining. Scale bar: A, C-G, 100 µm; B, 250 µm.

astrocytes and gemistocytes was performed using the human-specific marker HLA (human leukocyte antigen)-abc. In addition, HLA-abc staining clearly underlined the infiltrative intrahemispheric growth of U251 xenografts (Fig. 4B). FVIII-staining confirmed the florid angiogenetic processes (high microvessel density) associated with the peripherally infiltrating neoplastic projections (Table 2; Fig. 4D). Only occasional FVIII-positive intratumoral vascular channels were observed in U251 orthotopic xenografts (Table 2). Multifocal groups of active caspase-3-positive apoptotic cells, mostly concentrated in the necrotic and perinecrotic areas, were observed (Fig. 4E). Scattered apoptotic cells were also found in the viable neoplastic portions. Almost the entire U251 neoplastic cell population (96,51%) displayed a prominent nuclear accumulation of p53 protein (Table 2; Fig. 4F). Fifty-two % of U251 neoplastic cells also showed nuclear Ki-67 expression (Table 2). Multifocal HIF-1α nuclear expression by U251 neoplastic cells was recorded within pseudopalisades along the perinecrotic areas, as well as in the surrounding viable portion of the tumor (Table 2; Fig. 4G). For the vast majority of U251 neoplastic cells, pAkt-immunohistochemical analysis revealed a diffuse, finely granular positivity both in the cytoplasm and along the cell membrane (Fig. 6A).

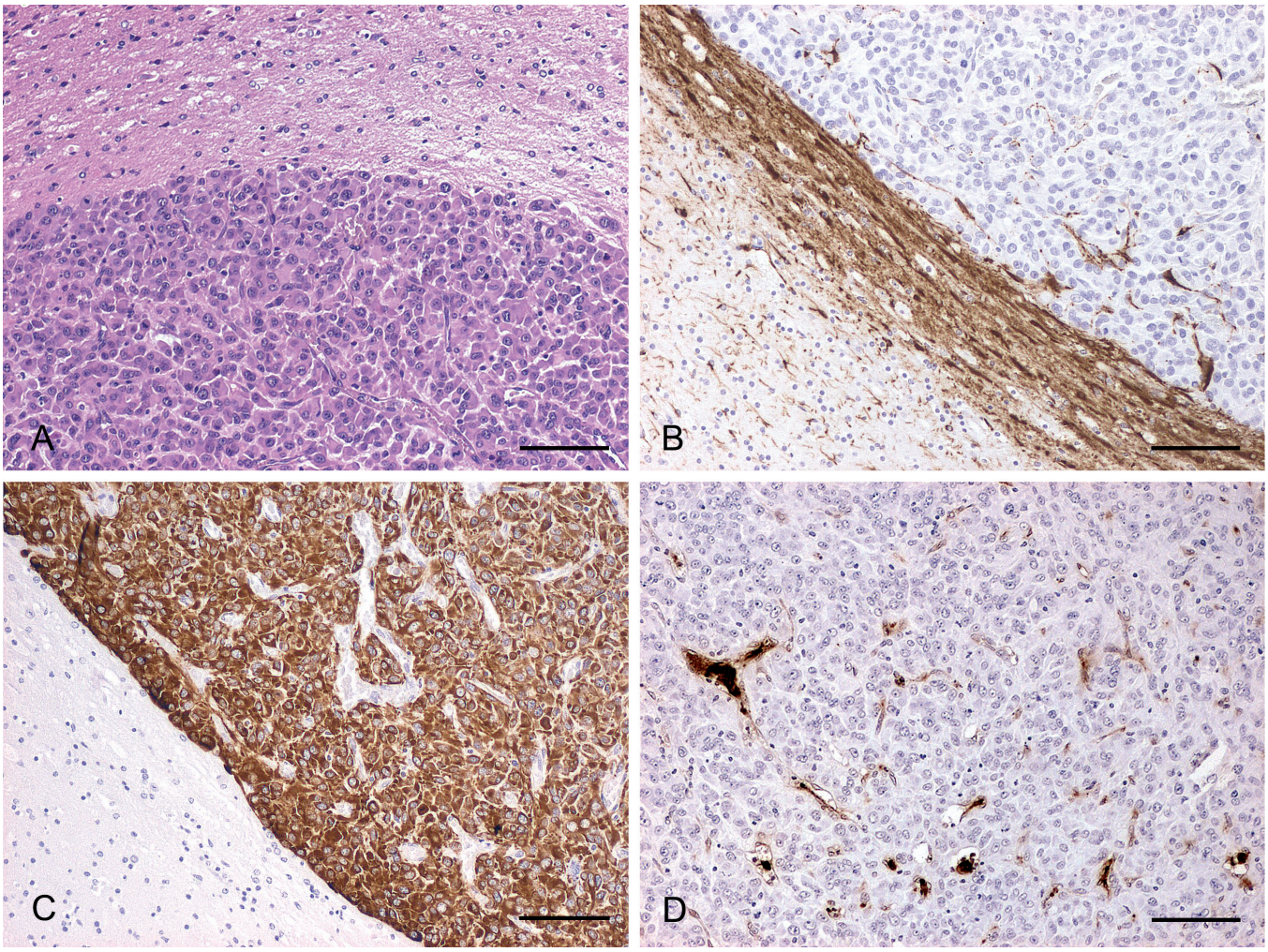

Fig. 5. Histopathology and immunohistochemistry of murine intracranial orthotopic xenograft of glioblastoma multiforme using U87MG human cell line. **A.** U87MG xenograft appears as well-demarcated intrahemispheric expansile mass consisting of tightly packed sheets of round to polygonal, occasionally plump spindle cells with abundant intensely eosinophilic cytoplasm. HE staining. **B.** U87MG xenograft result GFAP-negative and it is rimmed by a prominent GFAP-positive capsular reaction of astrogliosis. GFAP immunostaining. **C.** The human-specific marker HLA-abc highlights the intrahemispheric expansile growth of U87MG xenograft. HLA-abc immunostaining. **D.** The widespread intratumoral network of anastomosing vascular lacunae show an incomplete FVIII-positive endothelial lining. Furthermore, FVIII-staining highligts a large number of non-occlusive vascular microthrombi. FVIII immunostaining. Scale bar: 100 μm.

U87MG orthotopic xenografts were morphologically characterized by a single, densely cellular, well demarcated, non-infiltrating, expansile, intrahemispheric nodular mass surrounded by a compact reaction of astrogliosis. The mass consisted of tightly packed sheets of plump, round to polygonal, occasionally spindle cells with abundant intensely eosinophilic cytoplasm and frequent giant and multinucleated elements (Fig. 5A). Moderate findings of atypia were observed among neoplastic cell. These included anisocytosis, anysokariosis, bizarre mitosis and multiple irregular nucleoli. Variable-sized intratumoral foci of coagulative necrosis were observed in only two cases (Table 2). These were associated with prominent vascular thrombosis and concurrent marked neutrophilic infiltration. Neoplastic sheets were often separated by delicate anastomosing vascular lacunae and variable degrees of edema. Occasional intratumoral and peritumoral haemorrhagic foci were also observed.

In U87MG orthotopic xenografts, almost all the neoplastic cells displayed intense vimentin expression. On the contrary, no concurrent GFAP or S100 expression was recorded. Striking GFAP-expression was observed in the compact rim of reactive astrogliosis that surrounded neoplastic structures (Fig. 5B). A diffuse synaptophysin expression was observed in bearing brain parenchyma but not in U87MG neoplastic cells. Also, in these cases, the use of the human-specific marker HLA-abc allowed an accurate distinction between U87MG neoplastic astrocytes and murine reactive astrocytes/gemistocytes. In addition, human-specific HLA-abc antibody staining clearly underlined the expansile intrahemispheric growth of U87MG xenografts (Fig. 5C). FVIII-staining confirmed the presence of a high intratumoral microvessel density, consisting of a widespread network of anastomosing vascular lacunae. Furthermore, FVIII-staining delineated a large number of non-occlusive vascular microthrombi (Table 2; Fig. 5D). Only occasional FVIII-positive peritumoral vascular channels were observed in U87MG orthotopic xenografts (Table 2). Numerous groups of active caspase-3-positive apoptotic cells, mostly concentrated in the occasional necrotic and perinecrotic areas, were observed. Scattered apoptotic cells were also found in the viable neoplastic portions. Only 12,88% of the U87MG neoplastic cell population displayed variable degrees of p53-nuclear expression (Table 2). About 44% of U87MG cells showed nuclear Ki-67 expression (Table 2). HIF-1α nuclear expression by U87MG neoplastic cells was mostly distributed along the occasional perinecrotic areas (Table 2). For the vast majority of U87MG cells, pAkt immunohistochemical analysis revealed a diffuse, finely granular positivity, both in the cytoplasm and along the cell membrane (Fig. 6B).

Statistical analyses revealed significant differences between U251 and U87MG groups with respect to the peripheral (p=0,0079) and the central (p=0,0079) microvessel density (FVIII-immunostaining; Table 2). A significant difference between the two groups was also observed for p53- (p=0,0001) but not for Ki-67-immunopositive cells (p=0,2) (Table 2).

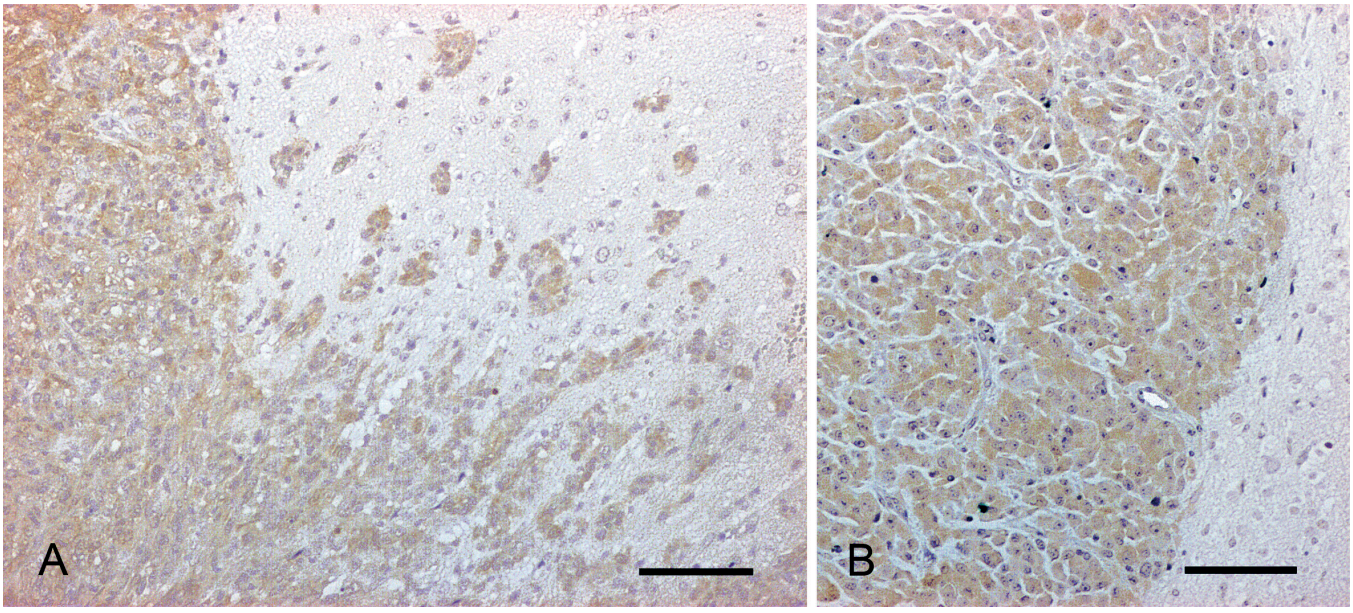

Fig. 6. Murine intracranial xenograft models of glioblastoma multiforme using U251 and U87MG human cell lines. Both U251 **(A)** and U87MG **(B)** tumor cells show diffuse, finely granular positivity for pAkt within the cytoplasm and along the cell membrane. pAkt immunostaining. Scale bar: 100 μm.

Discussion

In this study, the histopathological, immunohistochemical and MRI characterization highlighted profound differences between the two investigated orthotopic xenograft models of GBM. Indeed, where the U251 orthotopic xenograft model recapitulates most of the salient pathobiological features described in human spontaneous GBM, the U87MG orthotopic xenograft model proved to be very different.

MR imaging monitoring of U251 orthotopic xenografts was able to detect the progressive invasive growth into the surrounding brain parenchyma, the development of intratumoral necrotic areas, as well as the peripheral florid vascular activity with edema. Similar imaging findings are also reported for human GBM, and are considered important diagnostic and prognostic features (Rong et al., 2006). In U251 xenografts, the nature of signal alterations observed on MRI was then confirmed through the histopathological and immunohistochemical examination.

Neoplastic cells in U251 orthotopic xenografts showed a typical GBM phenotype, staining concurrently positive for vimentin, GFAP, S100 and negative for synaptophysin (Kleihues et al., 2000; Porter et al., 2004). In agreement with the striking interhemispheric invasive spread reported for human spontaneous GBM, in this study, HLA-abc staining precisely defined the prominent infiltrative behaviour of the growing U251 xenograft and its tendency to invade the ventricular system (Kleihues et al., 2000).

In U251 orthotopic xenografts, intratumoral areas of coagulative necrosis, similar to that described for human spontaneous GBM, displayed a serpiginous morphology and were peculiarly lined by pseudopalisading neoplastic cells. The coagulative nature and the serpiginous morphology of the necrotic areas suggest an underlying vascular damage with ischemic process (Zagzag et al., 2000a; Brat et al., 2004). In human GBM, the activation of a prothrombotic state along neoplastic vasculature is considered one of the most likely causes of ischemic necrosis. However, the molecular mechanisms promoting this peculiar event are largely unclear (Brat and Van Meir, 2004). In U251 xenografts neither histopathological examination or FVIII-staining were able to detect necrosis-associated occlusive thrombotic lesions. This finding indicates that vascular thrombosis does not represent the mechanisms leading to pseudopalisading necrosis in this model. However, other mechanisms such as vascular collapse and marked CD95-CD95 ligand-mediated apoptotic activity should be considered in the pathogenesis of GBM pseudopalisading necrosis (Tachibana et al., 1996; Kleihues et al., 2000; Brat and Van Meir, 2004). In U251 orthotopic xenografts, a prominent active caspase-3 signal was indeed observed along pseudopalisades and within the cellular debris in necrotic areas. A similar immunohistochemical distribution of active caspase-3 has been described in human spontaneous GBM as well as in murine subcutaneous xenografts using U251 cell line (Ray et al., 2002; Gdynia et al., 2007). These findings may indicate that not only in human GBM but also in U251 xenograft models, the apoptotic pathway plays a remarkable role in the formation of pseudopalisading necrosis. In addition, recent in vitro and in vivo observations indicated that in glioblastoma cells, constitutive caspase-3 activity promotes migration and invasiveness in a CD95/CD95 ligand independent manner (Gdynia et al., 2007). U251 intracranial model could be therefore proposed as a reasonable preclinical tool to test the efficacy of caspase-3 inhibition as a novel strategy for the treatment of glioblastomas.

In U251 orthotopic xenografts, the pattern of angiogenesis was characterized by florid microvascular proliferations along the neoplastic infiltrative projections. This latter finding represents a common feature in naturally occurring human GBM (Homma et al., 2006). In these xenografts, pseudopalisading necrosis, microvascular proliferations and neoplastic invasion of the adjacent brain parenchyma represent strictly interconnected features (Brat and Van Meir, 2004). Furthermore, as reported for most of the human spontaneous GBM, these features are associated with widespread HIF-1α expression along pseudopalisades, as well as in the viable portion of the tumor (Zagzag et al., 2000b, 2006). Taken together, these aspects suggest that human spontaneous GBM and this model share the same unique pathophysiological mechanisms that link necrosis and hypoxia to microvascular proliferations and invasive behaviour (Rong et al, 2006). For this reason, the U251 orthotopic mouse model could be efficaciously employed in the study of compounds that target HIF-1α downstream signalling pathway.

TP53 is known to be mutated in most of the secondary human GBM and also in lower grade precursor astrocytic tumors. Furthermore, immunohistochemical examination demonstrated that mutation of TP53 in secondary GBM generally leads to a nonfunctional p53 protein accumulation within nuclei of neoplastic cells (Kleihues et al., 2000; Ganigi et al., 2005; Brat et al., 2007). The same pattern of expression was observed for the U251 orthotopic xenograft model, where p53 immunostaining revealed a marked nuclear staining in almost the entire neoplastic cell population. The U251 cell line is known to harbour mutated TP53 (Lang et al., 1998). Several studies have demonstrated that GBM harbouring TP53 mutation and non fuctional p53 may exhibit a specific spectrum of susceptibility to adjuvant therapy and different postsurgical outcomes (Lang et al., 1998; Matsumoto, 1998; Shih et al., 2005). For the reasons mentioned above, the U251 orthotopic mouse model could be proposed as a reasonable preclinical tool to test the efficacy of novel adjuvant therapy protocols designed for TP53-mutated GBM.

For the vast majority of the examined features, the U87MG orthotopic xenograft model proved to be very

dissimilar from both the U251 orthotopic xenograft model and human spontaneous GBM. MR imaging monitoring of U87MG xenografts detected a progressively expansile, non-infiltrating regularly growing mass (tennis ball appearance) without consistent evidence of intratumoral necrosis, microvascular proliferation and invasiveness. All these aspects were then confirmed through the histopathological and immunohistochemical examination of serial coronal sections of the whole cranium. U87MG orthotopic xenograft cells showed a vimentin-positive, GFAP and S100-negative phenotype that barely fits with spontaneous GBM phenotype (Kleihues et al., 2000; Porter et al., 2004). Another unusual finding in spontaneous human GBM, but always detected in U87MG xenografts, is represented by a complete and well-organized GFAP positive astroglial capsular reaction, limiting tumor growth and extension into the surrounding brain parenchyma.

In U87MG orthotopic xenografts the pattern of angiogenesis, characterized by a delicate intratumoral network of anastomosing vascular lacunae, is completely different when compared to the florid microvascular proliferations described in the U251 orthotopic model and in spontaneous human GBM. Although numerous fibrin thrombi were observed lodging in the vascular lacunae of U87MG orthotopic xenografts, occlusive events with consequent ischemic phenomena were uncommon. Unlike U251 xenografts, necrotic areas in U87MG model did not display the peculiar pseudopalisading morphology, and they were not associated with any other findings typical of high grade astrocytic tumor, such as pheripheral microvascular proliferation and invasive behaviour (Rong et al., 2006). Necrosis was also accompanied by a concurrent marked neutrophilic infiltration that represents an uncommon feature in spontaneous human GBM (Rong et al., 2006). For the reasons mentioned above, necrosis in U87MG xenografts should be considered an incidental finding, lacking any pathobiological analogies with necrotic lesions in spontaneous human GBM.

In U87MG xenografts, HIF-1α expression was observed in perinecrotic neoplastic cells. This pattern of distribution is quite similar to that reported for human GBM (Rong et al., 2006). However, the non-palisading morphology, as well as the inconsistency of the intratumoral necrosis in U87MG xenografts, make the pathobiological value of this finding not comparable with the human counterpart.

U87MG cells are known to be TP53 wild type (Lang et al., 1998; Clark et al., 2007; Trog et al., 2007). This aspect was also confirmed in this study, where U87MG orthotopic xenografts exhibited a typical p53 wild type immunhistochemical pattern with only 13% of neoplastic cells showing different intensity of expression.

Although it is still a matter for debate, several studies have demonstrated that in spontaneous GBM, Ki-67 expression is directly correlated with aggressive behaviour and poor prognosis (Torp, 2002; Kleinschmidt-DeMasters et al., 2006). In this study, both the orthotopic models examined exhibited elevated levels of Ki-67 expression and no significant differences were observed.

As expected for both cell lines studied, orthotopic xenografts displayed a diffuse pAkt-expression (Zinda et al., 2001; de la Peña et al., 2006; Zhang et al., 2007). In GBM, EGFR overexpression-amplification and PTEN mutation represent the two major genetic abnormalities accounting for the constitutive activation of PI3K/Akt signalling pathway. These events result in cell proliferation, increased cell survival and resistance to radiation (Pelloski et al., 2006). For this reason, for both the GBM xenograft models investigated, immunohistochemical monitoring of pAkt-expression may represent a useful tool in preclinical studies of compounds specifically targeting EGFR overexpression-amplification and PTEN mutation.

In conclusion, this study demonstrates that the U251 orthotopic xenograft mouse model may be proposed as a predictive and reliable tool to target human GBM in preclinical studies, since it recapitulates most of the salient pathobiological features reported for human spontaneous GBM.

Acknowledgements. The authors thank Dr Vanessa Marchesi for the English revision of the manuscript

References

Brat D.J. and Van Meir E.G. (2004). Vaso-occlusive and prothrombotic mechanisms associated with tumor hypoxia, necrosis, and accelerated growth in glioblastoma. Lab. Invest. 84, 397-405.

Brat D.J., Castellano-Sanchez A., Kaur B. and Van Meir E.G. (2002). Genetic and biologic progression in astrocytomas and their relation to angiogenic dysregulation. Adv. Anat. Pathol. 9, 24-36.

Brat D.J., Castellano-Sanchez A.A., Hunter S.B., Pecot M., Cohen C., Hammond E.H., Devi S.N., Kaur B. and Van Meir E.G. (2004). Pseudopalisades in glioblastoma are hypoxic, express extracellular matrix proteases, and are formed by an actively migrating cell population. Cancer Res. 64, 920-927.

Brat D.J., Shehata B.M., Castellano-Sanchez A.A., Hawkins C., Yost R.B., Greco C., Mazewski C., Janss A., Ohgaki H. and Perry A. (2007). Congenital glioblastoma: a clinicopathologic and genetic analysis. Brain Pathol. 17, 276-281.

Candolfi M., Curtin J.F., Nichols W.S., Muhammad A.G., King G.D., Pluhar G.E., McNiel E.A., Ohlfest J.R., Freese A.B., Moore P.F., Lerner J., Lowenstein P.R. and Castro M.G. (2007). Intracranial glioblastoma models in preclinical neuro-oncology: neuropathological characterization and tumor progression. J. Neurooncol. 85, 133-148.

Clark A.J., Chan D.C., Chen M.Y., Fillmore H., Dos Santos W.G., Van Meter T.E., Graf M.R. and Broaddus W.C. (2007). Down-regulation of Wilms' tumor 1 expression in glioblastoma cells increases radiosensitivity independently of p53. J. Neurooncol. 83, 163-172.

de la Peña L., Burgan W.E., Carter D.J., Hollingshead M.G., Satyamitra M., Camphausen K. and Tofilon P.J. (2006). Inhibition of Akt by the alkylphospholipid perifosine does not enhance the radiosensitivity of human glioma cells. Mol. Cancer Ther. 5, 1504-1510.

Fomcheenko E.I. and Holland E.C. (2006). Mouse models of brain tumors and their applications in preclinical trials. Clin. Cancer Res. 12, 5288-5297.

Ganigi P.M., Santosh V., Anandh B., Chandramouli B.A. and Sastry Kolluri V.R. (2005). Expression of p53, EGFR, pRb and bcl-2 proteins in pediatric glioblastoma multiforme: a study of 54 patients. Pediatr. Neurosurg. 41, 292-299.

Gdynia G., Grund K., Eckert A., Böck B.C., Funke B., Macher-Goeppinger S., Sieber S., Herold-Mende C., Wiestler B., Wiestler O.D. and Roth W. (2007). Basal caspase activity promotes migration and invasiveness in glioblastoma cells. Mol. Cancer. Res. 5, 1232-1240.

Goldbrunner R.H., Bendszus M., Sasaki M., Kraemer T., Plate K.H., Roosen K. and Tonn J.C. (2000). Vascular endothelial growth factor-driven glioma growth and vascularization in an orthotopic rat model monitored by magnetic resonance imaging. Neurosurgery 47, 921-929.

Henson J.W., Gaviani P. and Gonzalez R.G. (2005) MRI in treatment of adult gliomas. Lancet Oncol. 6, 167-175.

Homma T., Fukushima T., Vaccarella S., Yonekawa Y., Di Patre P.L., Franceschi S. and Ohgaki H. (2006). Correlation among pathology, genotype, and patient outcomes in glioblastoma. J. Neuropathol. Exp. Neurol. 65, 846-854.

Kaur B., Tan C., Brat D.J., Post D.E. and Van Meir E.G. (2004) Genetic and hypoxic regulation of angiogenesis in gliomas. J. Neurooncol. 70, 229-243.

Kleihues P., Burger P.C., Collins V.P., Newcomb E.W., Ohgaki H. and Cavenee W.K. (2000). Glioblastoma. In: World Health Organization Classification of Tumours. Pathology and genetics of tumours of the nervous system. Kleihues P. and Cavenee W.K. (eds). IARC Press, Lyon. pp 29-47.

Kleinschmidt-DeMasters B.K., Meltesen L., McGavran L. and Lillehei K.O. (2006). Characterization of glioblastomas in young adults. Brain Pathol. 16, 273-286.

Lang F.F., Yung W.K., Raju U., Libunao F, Terry N.H. and Tofilon P.J. (1998). Enhancement of radiosensitivity of wild-type p53 human glioma cells by adenovirus-mediated delivery of the p53 gene. J. Neurosurg. 89, 125-132.

Martínez-Murillo R. and Martínez A. (2007). Standardization of an orthotopic mouse brain tumor model following transplantation of CT-2A astrocytoma cells. Histol. Histopathol. 22, 1309-1326.

Matsumoto R. (1998). Clinical and pathological significance of p53 gene mutation in human cerebral glioblastoma multiforme. Hokkaido Igaku Zasshi. 73, 407-417.

Mischel P.S., Nelson S.F. and Cloughesy T.F. (2003). Molecular analysis of glioblastoma: pathway profiling and its implications for patient therapy. Cancer Biol. Ther. 2, 242-247.

Ohgaki H. and Kleihues P. (2007). Genetic pathways to primary and secondary glioblastoma. Am. J. Pathol. 170, 1445-1453.

Pelloski C.E., Lin E., Zhang L., Yung W.K., Colman H., Liu J.L., Woo S.Y., Heimberger A.B., Suki D., Prados M., Chang S., Barker F.G. 3rd, Fuller G.N. and Aldape K.D. (2006). Prognostic associations of activated mitogen-activated protein kinase and Akt pathways in glioblastoma. Clin. Cancer Res. 12, 3935-3941.

Pennacchietti S., Michieli P., Galluzzo M., Mazzone M., Giordano S. and Comoglio P.M. (2003). Hypoxia promotes invasive growth by transcriptional activation of the met protooncogene. Cancer Cell 3, 347-361.

Porter B.F., Summers B.A., Leland M.M .and Hubbard G.B. (2004). Glioblastoma multiforme in three baboons (Papio spp). Vet. Pathol. 41, 424-428

Preusser M., Haberler C. and Hainfellner J.A. (2006). Malignant glioma: neuropathology and neurobiology. Wien Med. Wochenschr. 156, 332-337.

Ray S.K., Patel S.J., Welsh C.T., Wilford G.G., Hogan E.L. and Banik N.L. (2002) Molecular evidence of apoptotic death in malignant brain tumors including glioblastoma multiforme: upregulation of calpain and caspase-3. J. Neurosci. Res. 15, 197-206.

Rong Y., Durden D.L., Van Meir E.G. and Brat D.J. (2006). 'Pseudopalisading' necrosis in glioblastoma: a familiar morphologic feature that links vascular pathology, hypoxia, and angiogenesis. J. Neuropathol. Exp. Neurol. 65, 529-539.

Shih H.A., Betensky R.A., Dorfman M.V., Louis D.N., Loeffler J.S. and Batchelor T.T. (2005). Genetic analyses for predictors of radiation response in glioblastoma. Int. J. Radiat. Oncol. Biol. Phys. 63, 704-710.

Tachibana O., Lampe J., Kleihues P. and Ohgaki H. (1996). Preferential expression of Fas/APO1 (CD95) and apoptotic cell death in perinecrotic cells of glioblastoma multiforme. Acta Neuropathol. 92, 431-434.

Torp S.H. (2002). Diagnostic and prognostic role of Ki-67 immunostaining in human astrocytomas using four different antibodies. Clin. Neuropathol. 21, 252-257.

Trog D., Moenkemann H., Breipohl W., Schueller H., Schild H. and Golubnitschaja O. (2007). Non-sufficient cell cycle control as possible clue for the resistance of human malignant glioma cells to clinically relevant treatment conditions. Amino Acids 32, 373-379.

Zagzag D., Amirnovin R., Greco M.A., Yee H., Holash J., Wiegand S.J., Zabski S., Yancopoulos G.D. and Grumet M. (2000a). Vascular apoptosis and involution in gliomas precede neovascularization: a novel concept for glioma growth and angiogenesis. Lab. Invest. 80, 837-849.

Zagzag D., Zhong H., Scalzitti J.M., Laughner E., Simons J.W. and Semenza G.L. (2000b). Expression of hypoxia-inducible factor 1 alpha in brain tumors: association with angiogenesis, invasion, and progression. Cancer 88, 2606-2618.

Zagzag D., Lukyanov Y., Lan L., Ali M.A., Esencay M., Mendez O., Yee H., Voura E.B. and Newcomb E.W. (2006). Hypoxia-inducible factor 1 and VEGF upregulate CXCR4 in glioblastoma: implications for angiogenesis and glioma cell invasion. Lab. Invest. 86, 1221-1232.

Zhang R., Banik N.L. and Ray S.K. (2007). Combination of all-trans retinoic acid and interferon-gamma suppressed PI3K/Akt survival pathway in glioblastoma T98G cells whereas NF-kappaB survival signaling in glioblastoma U87MG cells for induction of apoptosis. Neurochem. Res. 32, 2194-2202.

Zhu X.P., Li K.L., Kamaly-Asl I.D., Checkley D.R., Tessier J.J., Waterton J.C. and Jackson A. (2000) Quantification of endothelial permeability, leakage space, and blood volume in brain tumors using combined T1 and T2* contrast-enhanced dynamic MR imaging. J. Magn. Reson. Imaging 11, 575-585.

Zinda M.J., Vlahos C.J. and Lai M.T. (2001). Ceramide induces the dephosphorylation and inhibition of constitutively activated Akt in PTEN negative U87mg cells. Biochem. Biophys. Res. Commun. 280, 1107-1115.

Accepted February 9, 2009